metals

MDPI

Article

Microstructure and Mechanical Behavior of Al-Mg Composites Synthesized by Reactive Sintering

Rub Nawaz Shahid and Sergio Scudino *

Institute for Complex Materials, IFW Dresden, Helmholtzstraße 20, D-01069 Dresden, Germany; r.n.shahid@ifw-dresden.de

* Correspondence: s.scudino@ifw-dresden.de; Tel.: +49-351-4659-838

Received: 6 September 2018; Accepted: 19 September 2018; Published: 25 September 2018

Abstract: Lightweight metal matrix composites are synthesized from elemental powder mixtures of aluminum and magnesium using pressure-assisted reactive sintering. The effect of the reaction between aluminum and magnesium on the microstructure and mechanical properties of the composites due to the formation of β-Al_3Mg_2 and γ-$Al_{12}Mg_{17}$ intermetallics is investigated. The formation of the intermetallic compounds progressively consumes aluminum and magnesium and induces strengthening of the composites: the yield and compressive strengths increase with the increase of the content of intermetallic reinforcement at the expense of the plastic deformation. The yield strength of the composites follows the iso-stress model when the data are plotted as a function of the intermetallic content.

Keywords: metal matrix composites; phase transformation; intermetallics; powder metallurgy; ball milling; mechanical properties

1. Introduction

Developments in the production of energy efficient and environmentally friendly vehicles have shifted the interest of the transport industry from conventional structural materials to high-strength lightweight components [1–5]. The reduction of the weight of vehicles can enhance the fuel efficiency and limit greenhouse gas emissions, ultimately improving environmental protection [4–6]. Because of their remarkable properties, including a low density, high specific strength and stiffness, and improved deformability [7–12], aluminum and magnesium-based alloys and composites are evolving as potential replacements for conventional materials in the automobile, ship and aerospace industries; electronic products; and industrial equipment [13–18].

Particulate reinforced metal matrix composites (MMCs) are attractive due to their isotropic properties, easier processing routes and lower costs compared to the other metal matrix composites [19]. Various particulate reinforcements, such as ceramic [20,21], metallic glasses [22], quasicrystals [23,24], and complex metallic alloys [25] have been used to produce aluminum and magnesium-based matrix composites with enhanced properties through casting [26,27], metal infiltration [28,29], friction stir forming [30] and powder metallurgy [31–34].

Metallic reinforcements have several advantages over conventional reinforcing ceramic particulates, including easy and economical availability [35,36], improved recyclability of MMCs [37], better compatibility with a metallic matrix in terms of coefficient of thermal expansion and wettability [38–40], which may create a stronger interface between matrix and reinforcement [41]. The reaction between matrix and reinforcement can generate new phases during processing or post-processing heat treatment, thereby affecting the mechanical properties of the composite depending upon the volumetric changes associated with the transformation, nature of the new phases and their bonding with the surrounding material [8,42]. Such transformations may induce strengthening in MMCs, as, for example, reported

in composites consisting of an aluminum matrix reinforced with Al-Cu-Fe quasicrystals, where the reaction generates a new phase (the ω-Al_7Cu_2Fe) and increases the strength of the material [39,43]. In another example, the reaction between the Fe_3Al reinforcement and aluminum matrix produces two new phases (Al_5Fe_2 and $Al_{13}Fe_4$) that significantly enhance the strength of the composites [44]. Phase transformations due to the reaction between matrix and particulate reinforcements in the case of aluminum-magnesium matrix composites lead to the in-situ formation of several intermetallics, e.g., $Al_{12}Mg_{17}$, Al_3Mg_2, Al_2MgC_2, $MgAl_2O_4$, Al_3Ti, Ti_3B_4 [12,41,45], which has been reported as an effective way of composite strengthening along with other strengthening contributions.

Composite manufacturing through melting routes can lead to the heterogeneous distribution of the reinforcement due to agglomeration and segregation [46,47]. Furthermore, undesired and uncontrolled interfacial reactions between matrix and reinforcement can deteriorate the properties of the composites. Therefore, solid-state powder metallurgy represents a good choice among other processing techniques to produce near-net-shape products with uniformly dispersed reinforcements [48–51]. Powder metallurgy gives excellent control over the size, shape, distribution and volume fractions of the reinforcement and matrix, which, in turn, enables the creation of composites with desired microstructures and properties [52,53]. Furthermore, the extent of the interfacial reaction between matrix and reinforcement and the type of the reaction product(s) can be governed by properly controlling the process temperature [44,54,55].

The reaction between matrix and reinforcement achieved by powder metallurgy can be considered a type of reactive sintering, where the proper mixture of starting powders is sintered with or without the assistance of pressure in order to produce a variety of materials ranging from porous intermetallics or ceramics, crystallographic phase transformations, the formation of solid solutions and chemical compounds to nickel, and titanium aluminides and composites [56–64]. In this work, the reactive sintering of aluminum and magnesium elemental powder mixtures has been used to synthesize Al-Mg composites reinforced with Al_3Mg_2 and $Al_{12}Mg_{17}$ intermetallics formed in-situ during processing. The aim is to analyze the effect of the initial volume percent of magnesium on the microstructural modifications, in-situ formation of the intermetallic reinforcements and the resulting mechanical properties of the Al-Mg lightweight composites.

2. Materials and Methods

Commercially available aluminum and magnesium powders (–100 mesh) were blended by ball milling under an argon atmosphere for 1 h at a rotational speed of 100 rpm using a Retch PM 400 planetary ball mill (Retsch GmbH, Haan, Germany) with hardened steel balls and vials. To avoid a temperature rise during the blending process, milling was carried out for 15 min followed by rest intervals of 15 min. Powder mixtures with different amounts of Mg (V = 10, 20, 40, 60, 80, and 90 vol %) were hot-pressed under the argon atmosphere at 673 K by applying a uniaxial pressure of 640 MPa for 10 min. Additionally, to investigate the phase formation induced by the reaction between Al and Mg at different temperatures, aluminum, and magnesium bilayer specimens containing 50 vol % Mg were produced by hot pressing at 573, 623, and 673 K, while keeping the other hot pressing parameters constant (640 MPa pressure and 10 min holding time). The phases formed in the blended powders and hot-pressed composites were identified by X-ray diffraction (XRD) using a D3290 PANalytical X'pert PRO X-ray diffractometer (PANalytical, Almelo, The Netherlands) with Co $K\alpha$ radiation (λ = 0.179 nm). A scanning electron microscope GEMINI 1530 (Carl Zeiss NTS GmbH, Oberkochen, Germany) equipped with an energy dispersive X-ray spectrometer (EDX, Bruker AXS Microanalysis GmbH, Berlin, Germany) was used for microstructural characterization. Fifty to sixty scanning electron microscopy (SEM) micrographs were examined for every composite to estimate the volume fraction of the different phases by using the image analysis software: ImageJ (1.48v, National Institutes of Health, Bethesda, MD, USA). ImageJ counts the pixels of the highlighted phase to calculate its percentage based on a grayscale. The 'threshold' function is used to select the required phase by adjusting the upper and lower limits of the grayscale, then the 'analysis' function is used to count

the number of pixels present in the selected phase. The density of the hot-pressed composites was measured using the Archimedes method, giving an average relative density of the composites of 99 ± 0.3 g/cm^3. Cylindrical samples of 3 mm diameter and 6 mm length were prepared from the hot-pressed composites and then tested at room temperature under quasistatic compression using an Instron 5869 universal testing machine (strain rate = 8 × 10^{-5} s^{-1}, Instron, Norwood, MA, USA). A Fiedler laser-extensometer (Fiedler Optoelektronik GmbH, Lützen, Germany) was used to measure the sample strain. To ensure the reproducibility of the results, a minimum of four samples for each composite was tested. The compression tests were deliberately stopped at 20% strain for the composite containing 10 vol % Mg because of its high deformability.

3. Results and Discussion

3.1. Phase Analysis and Microstructural Characterization

Figure 1a shows the XRD patterns for the Al-Mg powder mixtures after 1 h of blending by ball milling. The patterns indicate the presence of pure aluminum and magnesium only, which illustrates the absence of any reaction during the mechanically-induced mixing process carried out in the present milling conditions. Aluminum and magnesium react during the hot consolidation of the powder mixtures at 673 K to create the β-Al_3Mg_2 and γ-$Al_{12}Mg_{17}$ intermetallics, as shown in Figure 1b. The XRD patterns for the consolidated composites with an initial content of 10 and 20 vol % Mg (V = 10 and 20) exhibit the presence of Al_3Mg_2 along with residual aluminum, whereas $Al_{12}Mg_{17}$ and magnesium are not observed. The composites with V = 40 and 60 contain both Al_3Mg_2 and $Al_{12}Mg_{17}$ accompanied by residual magnesium and aluminum. In contrast, the composites V = 80 and 90 show only the presence of $Al_{12}Mg_{17}$ and magnesium, while the Al_3Mg_2 and aluminum phases are not observed. The creation of Al_3Mg_2 and $Al_{12}Mg_{17}$ during the high-temperature processing of aluminum and magnesium composites is in compliance with the reported results [65–69].

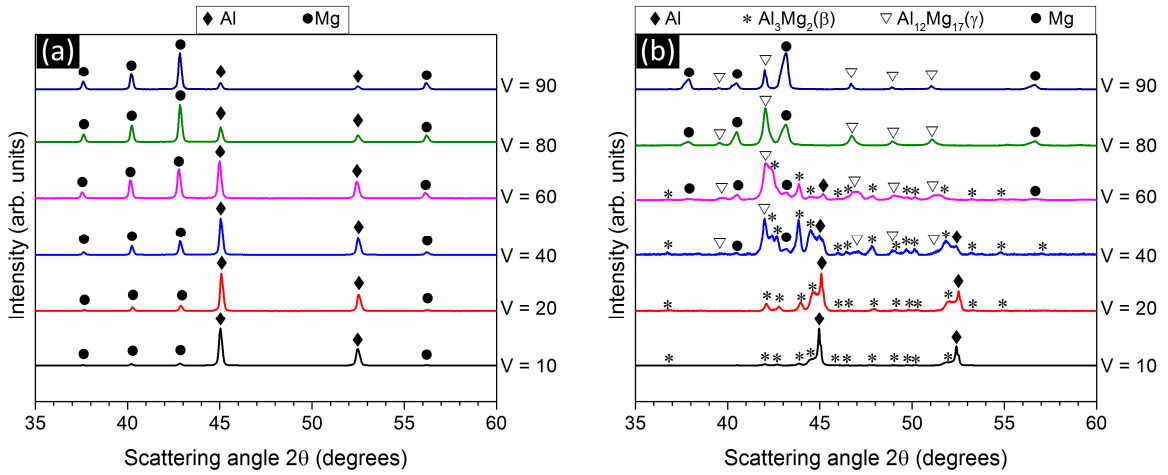

Figure 1. The X-ray diffraction (XRD) patterns (Co Kα radiation) of Al-Mg (**a**) powder mixtures milled for 1 h and (**b**) composites hot-pressed at 673 K. (V = 10, 20, 40, 60, 80, and 90 indicate the initial vol % of Mg).

The SEM images and EDX elemental maps and profiles for the consolidated composites are displayed in Figures 2–4. The composites with V = 10 and 20 show a core-shell microstructure that consists of a Mg core enclosed by two consecutive shells of $Al_{12}Mg_{17}$ and Al_3Mg_2 which are finally covered by a rather continuous residual aluminum (Figure 2). The formation of multiphase in-situ core-shell microstructures has been reported in several composite systems [41,70–75] and can be attributed to the incomplete transformation reactions under the current processing parameters, like temperature and pressure [44]. In the composite with V = 40, the continuity of the aluminum phase has been disrupted by the substantial growth of the intermetallics, resulting from the higher

initial volume percentage of magnesium. Here, the Al_3Mg_2 phase is continuous throughout the microstructure, the magnesium cores are surrounded by the $Al_{12}Mg_{17}$ phase, and only a limited amount of isolated Al is observed. In the composite V = 60 (Figure 3), the size of the isolated aluminum regions further decreases, while the size of the magnesium cores increases and both the Al_3Mg_2 and $Al_{12}Mg_{17}$ intermetallic phases are rather continuous throughout the microstructure. Conversely, in the composite V = 80, pure aluminum is not found and the Al_3Mg_2 phase appears as cores encapsulated by the $Al_{12}Mg_{17}$ phase, which is further covered by a continuous residual magnesium phase. The microstructure of the composite V = 90 consists of islands of $Al_{12}Mg_{17}$ phase surrounded by residual magnesium. Phase identification in the composites is supported by the EDX elemental concentration profiles shown in Figure 4, which are in good agreement with the XRD results in Figure 1b.

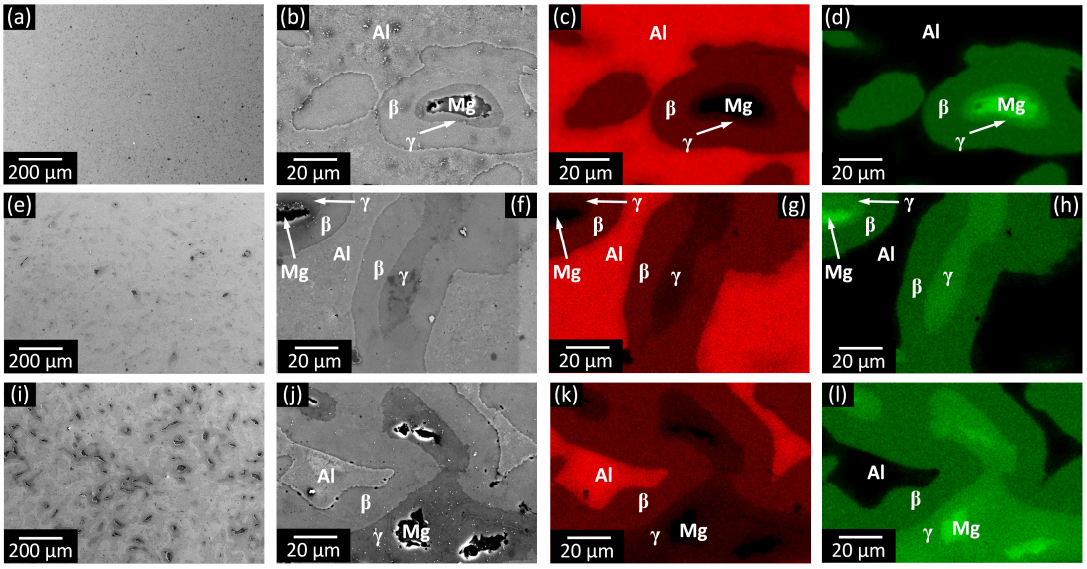

Figure 2. The SEM (scanning electron microscopy) images and EDX (energy dispersive X-ray spectrometry) elemental maps of the Al (red) and Mg (green) distributions for the Al-Mg composites hot-pressed at 673 K with an initial Mg content of (**a**–**d**) 10, (**e**–**h**) 20 and (**i**–**l**) 40 vol %.

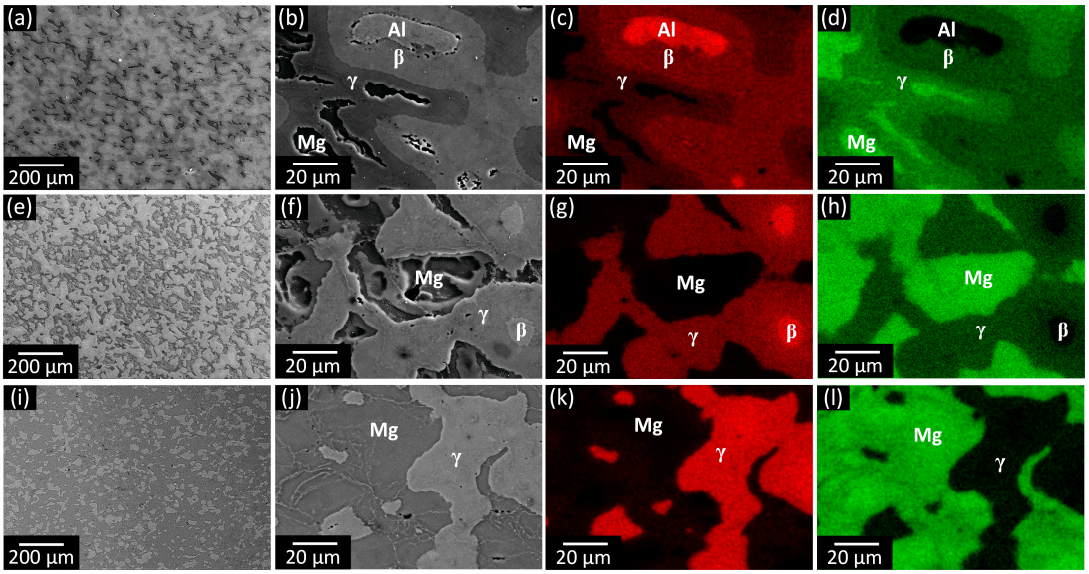

Figure 3. The SEM images and EDX elemental maps of the Al (red) and Mg (green) distributions for the Al-Mg composites hot-pressed at 673 K with an initial Mg content of (**a**–**d**) 60, (**e**–**h**) 80 and (**i**–**l**) 90 vol %.

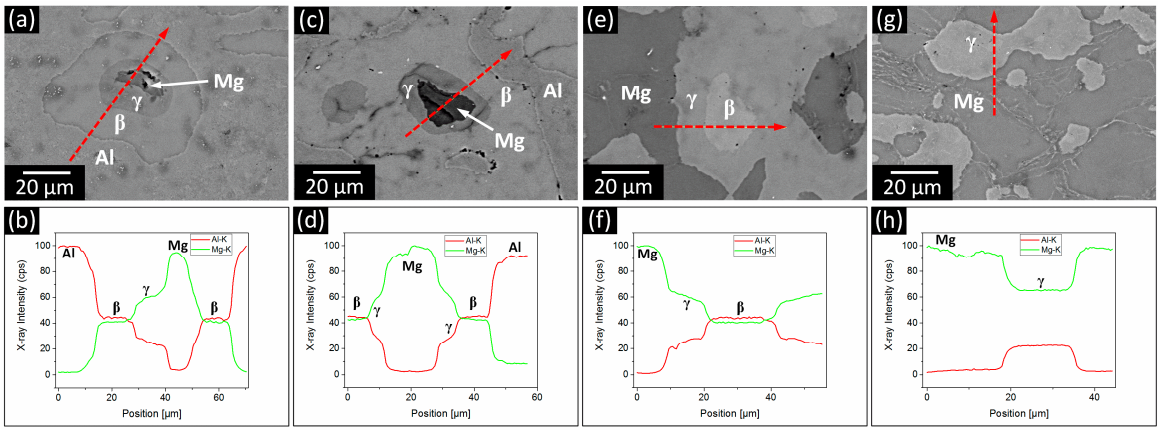

Figure 4. The SEM images and EDX elemental concentration profiles for the composites hot-pressed at 673 K with an initial magnesium content of (**a**,**b**) 10, (**c**,**d**) 40, (**e**,**f**) 80 and (**g**,**h**) 90 vol %. The dashed red arrows represent the scanned EDX line.

Figure 5 illustrates the volume percentages of the different phases in the consolidated composites, estimated from the SEM images, as a function of the initial volume content of magnesium (V). The quantity of Al_3Mg_2 progressively increased from ~15 vol % for V = 10 to ~55 vol % for V = 40. Afterward, it gradually declined to ~1.5 vol % for V = 80 and, finally, it was not present anymore in the composite with V = 90. The amount of $Al_{12}Mg_{17}$ slowly rose to ~12 vol % for V = 40, then sharply increased to 50 and 53 vol % for V = 60 and 80, respectively, and finally decreased to about 25 vol % for V = 90. The amount of aluminum decreased continuously from ~85% for V = 10 to ~3% for V = 60 and then it diminished to zero in the composites V = 80 and 90. The quantity of residual magnesium for V = 40 was ~2 vol % and then it steadily increased to ~75 vol % for V = 90. Figure 5 divides the consolidated composites into two sections separated by vertical lines on the basis of the volume profiles intersections. At about V = 55, the amount of aluminum and magnesium were equal. Additionally, the volume profiles of $Al_{12}Mg_{17}$ and Al_3Mg_2 also intersected at the same point. This suggests that the microstructure of the composites from V = 10 to 55 consist of aluminum as the major soft phase along with Al_3Mg_2 and $Al_{12}Mg_{17}$ as dominant reinforcements, whereas for V > 55, magnesium becomes the main soft phase predominantly reinforced by $Al_{12}Mg_{17}$, except for the composite with V = 60, where both $Al_{12}Mg_{17}$ and Al_3Mg_2 are present in high percentages.

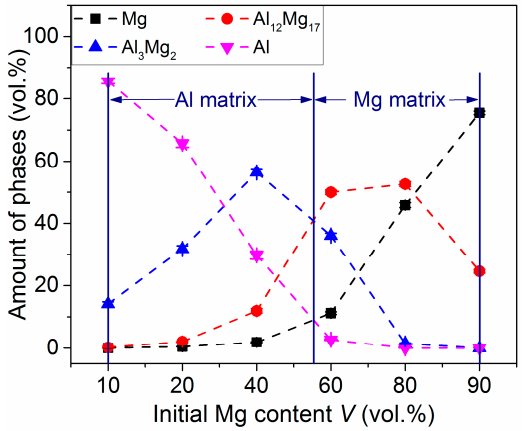

Figure 5. The variation of the amounts of the different phases present in the Al-Mg composites hot-pressed at 673 K.

3.2. Phase Formation During the Reaction of Al and Mg

In order to further examine the phase formation induced by the reaction between Al and Mg, aluminum and magnesium bilayer specimens were produced by hot pressing at different temperatures

(573, 623, and 673 K). The corresponding SEM images and EDX elemental concentration profiles across the interface between the Al and Mg layers are shown in Figure 6. In a homogenous composite, phase transformations occurring at an Al-Mg interface may have an influence on the diffusion and reaction fields arising from its neighboring similar interfaces. The synthesis of the bilayer composites helps to analyze the sequence of the intermetallics formation at the Al-Mg interface in the absence of any reactional caused by the neighboring interfaces. The Al-Mg bilayer composite hot-pressed at 573 K does not display any reaction product (Figure 6a–c). Because the diffusion coefficient of aluminum is higher than that of magnesium [76–78], it is plausible to assume that at a higher processing temperature (623 K) the aluminum atoms diffuse into the magnesium layer and form $Al_{12}Mg_{17}$ as the first reaction product (Figure 6d–f). The Al_3Mg_2 phase may then be generated by the additional diffusion of aluminum into the $Al_{12}Mg_{17}$ intermetallic and by the diffusion of magnesium into the Al matrix [79,80]. At this stage, the reaction is rather discontinuous and a rough layer of $Al_{12}Mg_{17}$ and Al_3Mg_2 intermetallics is formed at the Al-Mg interface. The interfacial layer is composed of a 3 ± 1 µm thick $Al_{12}Mg_{17}$ layer next to magnesium and a 4 ± 3 µm thick Al_3Mg_2 layer next to aluminum. The existence and position of both intermetallic layers at the Al-Mg interface observed here are in accordance with previous studies [81–85]. A further increase of temperature to 673 K smoothens the interface and enlarges the widths of the intermetallic layers to 5 ± 1 µm thick $Al_{12}Mg_{17}$ and 14 ± 1 µm thick Al_3Mg_2. The limited growth of the $Al_{12}Mg_{17}$ layer can be attributed to its smaller value of the inter-diffusion coefficient in comparison to Al_3Mg_2 [80,86].

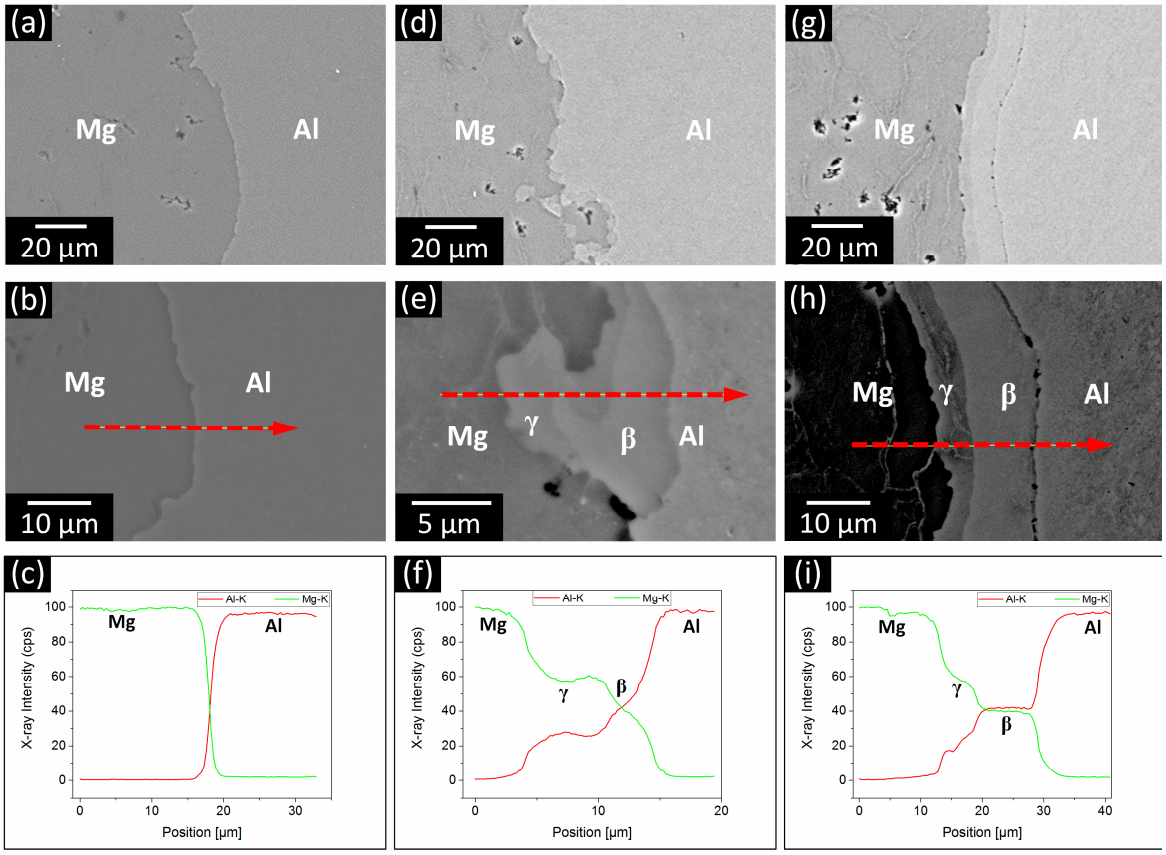

Figure 6. The SEM micrographs and EDX elemental concentration profiles for the bilayer Al-Mg composites hot-pressed at (**a**–**c**) 573, (**d**–**f**) 623 and (**g**–**i**) 673 K. The dashed red arrows represent the scanned EDX line.

A closer look at the interface of the bilayer hot-pressed at 623 K (Figure 7a) reveals additional features characterizing the surface of the aluminum layer. Every area on the aluminum surface undergoing the reaction with Mg is concave, whereas the intermetallics are hump-shaped islands with

a similar morphology throughout the specimen. As already mentioned, the diffusion coefficient of aluminum is one to two orders of magnitude higher than that of magnesium [77,87]. The aluminum atoms diffuse through the interface with a higher flux than that of magnesium and when the composition of the γ-$Al_{12}Mg_{17}$ intermetallic phase is locally reached, it nucleates and progressively grows into the magnesium layer [77,79,83]. The preferential formation of the intermetallic phases at the concave zones of the aluminum surface indicates that the stoichiometric concentration of aluminum atoms to form the intermetallics is reached faster in the concave zone than at the convex or straight zones. This aspect is schematically depicted in Figure 7b, which shows the linear paths of the diffusion of aluminum atoms in the Al-Mg bilayer. The diffusion line density in the concave zones is larger than that in the convex zones. As a result, the stoichiometric concentration in the concave zones is reached faster than in any other zone.

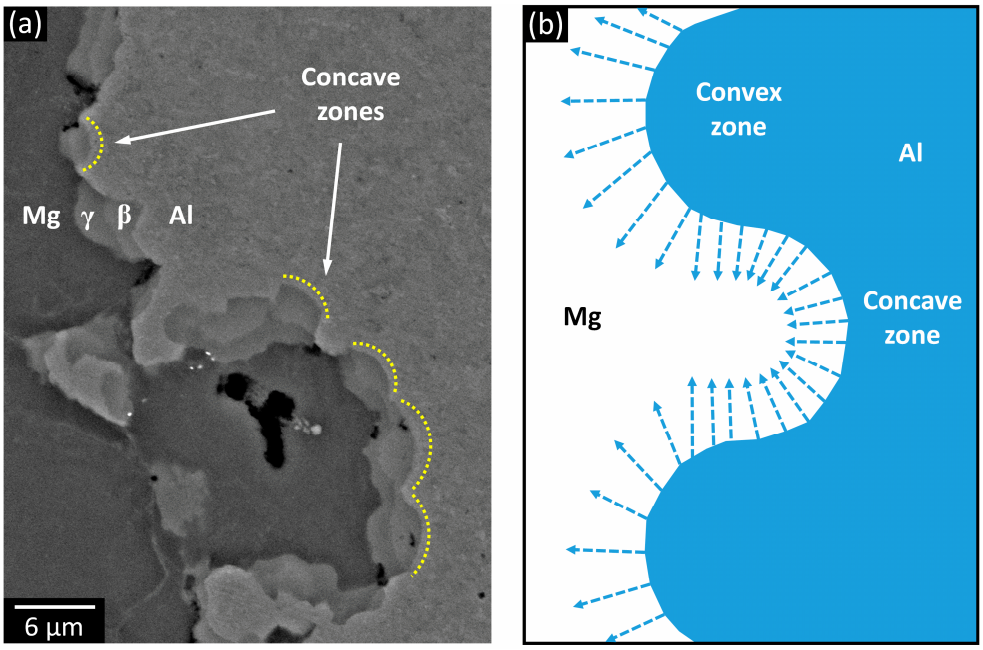

Figure 7. (**a**) The SEM image of the Al-Mg interface in the bilayer composite hot-pressed at 623 K showing the preferential formation of the intermetallic phases at the concave zones of the aluminum surface. (**b**) The schematic representation of the linear paths of the diffusion of aluminum atoms in the Al-Mg bilayer.

The bilayer composite hot-pressed at 673 K (Figure 8a) shows thicker layers of intermetallics. The Arrhenius diffusion equation predicts a higher atomic and vacancy mobility at higher temperatures [88], which, in turns, explains the larger thickness of the intermetallic phases compared with the material hot-pressed at 623 K. An oxide layer is present along the aluminum layer facing the edge of β-Al_3Mg_2. This oxide layer represents the initial contact surface between the aluminum and magnesium particles [77] and its existence near aluminum indicates that the phase transformations occur within the magnesium region [77]. The presence of the boundaries of the pre-existing magnesium particle in the γ-$Al_{12}Mg_{17}$ phase supports this conclusion (compare Figure 8a,b). The interfaces between Mg and γ-$Al_{12}Mg_{17}$ and between γ-$Al_{12}Mg_{17}$ and β-Al_3Mg_2 do not show porosity, while the interface between β-Al_3Mg_2 and Al exhibits porosity that can be designated as Kirkendall's porosity [89]; this aspect can be ascribed to the higher mobility of aluminum atoms in comparison to magnesium and to the coalescence of vacancies towards aluminum [76,77,90].

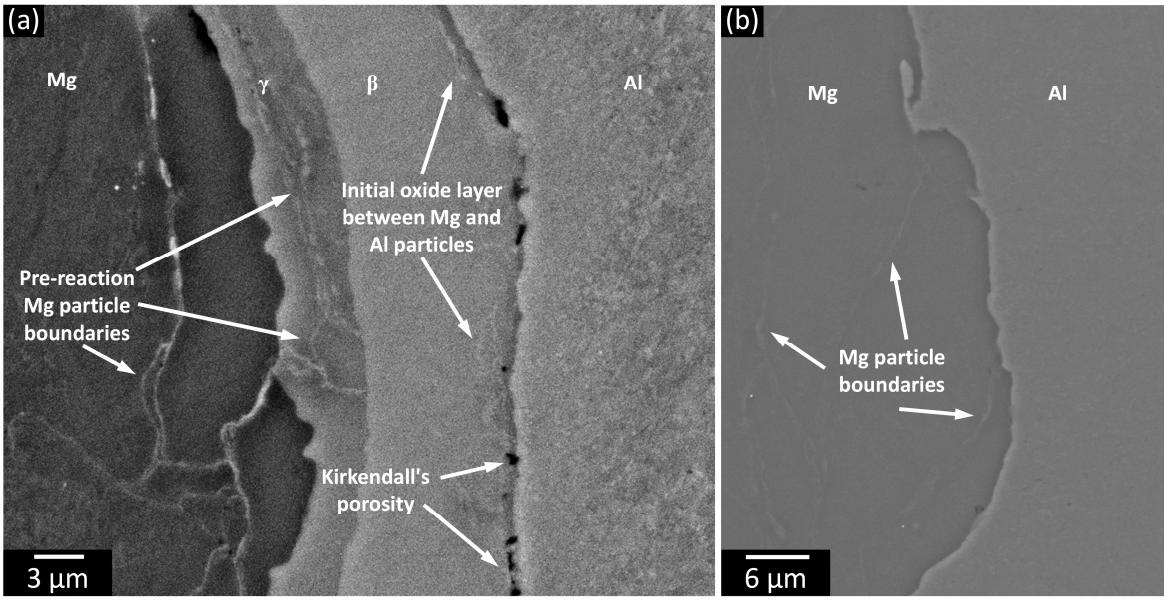

Figure 8. The SEM images of the Al-Mg interface in the bilayer composite hot-pressed at (**a**) 673 and (**b**) 573 K.

3.3. Mechanical Properties

Figure 9a,b display the room temperature compression stress-strain curves for the composites and the summary of the corresponding mechanical data. The yield strength (0.2% offset) of the composites increases from 126 ± 7 MPa for the material with V = 10 to 562 ± 23 MPa for the composite V = 60 and then decreases to 207 ± 20 MPa for the composite V = 90. Similarly, the compressive strength (the maximum stress that a material can stand under compression loading [91]) increases from 238 ± 7 MPa for the composites with V = 10 to 562 ± 23 MPa for V = 60, and afterward it decreases to 385 ± 20 MPa for the composites with V = 90. Conversely, the plastic deformability of the composites drastically decreases from 17% ± 0.2% to 1.2% ± 0.1% for the composites with V = 20 and 60, then it increases again to 11 ± 0.3% for the composite V = 90. The composite with V = 10 does not show failure up to the 20% strain, where the test was stopped. The yield strength of the composites cannot be directly correlated to the initial volume percentage of magnesium, as shown in Figure 9c. The in-situ formed Al_3Mg_2 and $Al_{12}Mg_{17}$ intermetallics are the reinforcing phases in the present composites. Therefore, the yield strength data are plotted in Figure 9d as a function of the cumulative amount of both intermetallics along with the strength values predicted by the iso-stress (red dashed lines) and iso-strain (blue dot-dashed line) models of the rule of mixture (RoM) [92–94]. The yield strength of the composites increases with increasing the total amount of intermetallics. The values of strength are closer to the iso-stress model, which assumes that the matrix and reinforcement experience the same stress during deformation, while the iso-strain model, which assumes that all components of a composite undergo the same strain during deformation [93], overestimates the values. Under compressive loading, the reinforcement particles move in the loading direction to get closer to each other if the volume fraction of reinforcement is high and the distance between the reinforcement particles is small [95]. In such cases, the reinforcement particles may undergo deformation due to load transfer and the strength of the composites follows the iso-strain model [95]. On the other hand, a smaller volume fraction of reinforcement leads to a larger distance between reinforcement particles and, in such cases, deformation takes place mainly in the matrix. The iso-stress model describes the strength behavior of this type of composite [95–97]. Therefore, the deviation of the yield strength data for the composites with V = 40, 60 and 80 could be attributed to the high volume fraction of the reinforcement and complex microstructure. The iso-stress behavior for aluminum matrix composites and the deviation of the yield strength from it have been observed in previous studies [44,92,97,98].

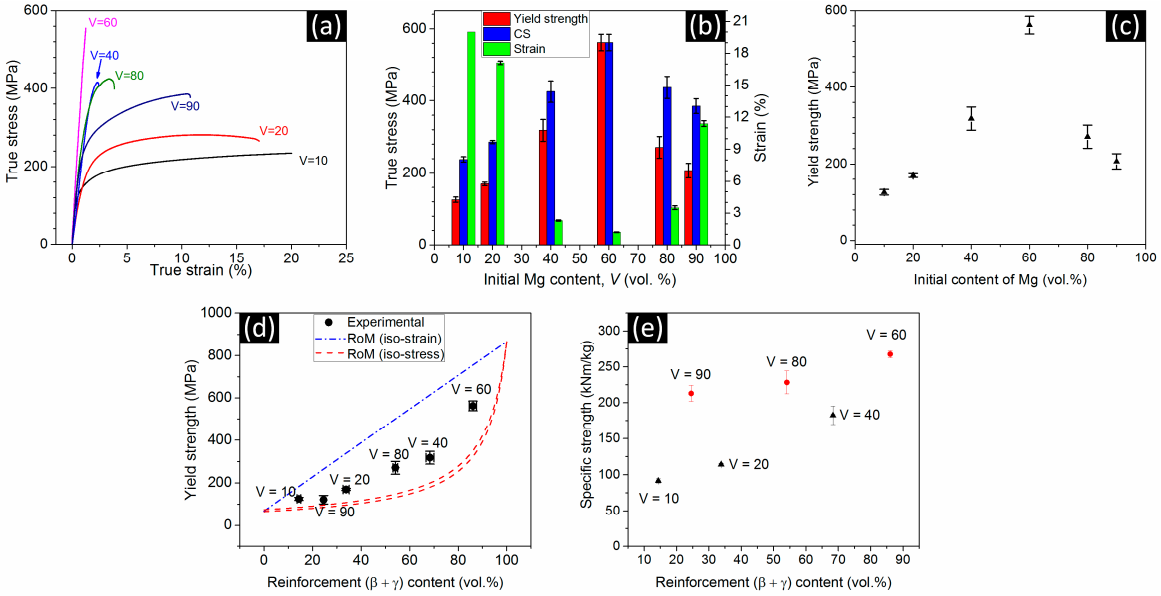

Figure 9. (**a**) The room temperature compression stress-strain curves for the composites with V = 10, 20, 40, 60, 80, and 90 hot-pressed at 673 K and (**b**) summary of the mechanical data. (**c**) Yield strength of the composites as a function of the initial Mg content (V). (**d**) Experimental yield strength of the composites as a function of the cumulative amount of β-Al_3Mg_2 and γ-$Al_{12}Mg_{17}$ and values calculated using the iso-stress and iso-strain models. The red dashed curves in (**d**) correspond to the iso-stress models with the Mg (lower curve) and Al (upper curve) matrices. The yield strength for the 100 vol % Al_3Mg_2 + $Al_{12}Mg_{17}$ in (**d**) is calculated from their hardness values given in References [99,100]. (**e**) Specific strength (compressive strength divided by the density) of the composites as a function of the amount of β-Al_3Mg_2 + γ-$Al_{12}Mg_{17}$.

Finally, Figure 9e shows the specific strength (compressive strength divided by the density) of the composites vs. the cumulative volume percent of the β-Al_3Mg_2 and γ-$Al_{12}Mg_{17}$ reinforcement. The specific strength of the composites with aluminum as a major soft phase is represented by black triangles, while, in the case of magnesium as the main phase, red circles are used. The specific strength of pure aluminum (55 kN m kg^{-1} [101]) increases to 90 and 180 kN m kg^{-1} by adding only 10 and 40 vol % of magnesium as a result of the creation of approximately 14 and 67 vol % intermetallics. Similarly, the specific strength of the composites with magnesium as the main soft phase, containing 25 (V = 90) and 85 vol % (V = 60) of intermetallics increases from 210 to 270 kN m kg^{-1}, respectively. These results are in line with the data reported for Al-based composites reinforced with β-Al_3Mg_2 particles [101] and indicate that lightweight composites with a wide range of strength and plastic deformation can also be successfully synthesized by the reactive sintering of the proper elemental powder mixtures. This processing route represents an additional degree of freedom in the development of lightweight materials with designed mechanical and physical properties able to meet specific requirements.

4. Conclusions

The reactive hot consolidation of Al-Mg powder mixtures has been used to synthesize lightweight composites reinforced with β-Al_3Mg_2 and γ-$Al_{12}Mg_{17}$ intermetallics formed in-situ during consolidation. Detailed microstructural characterization and comprehensive phase analysis have been employed to examine the morphology of the phases in the composites and to achieve their identification and quantification. The formation of core-shell microstructures is observed in the Al-rich composites, where the Mg cores are surrounded by a double-shell of β-Al_3Mg_2 and γ-$Al_{12}Mg_{17}$ intermetallic phases. In the Mg-rich composites, aluminum has been fully consumed except in the composite V = 60. Microstructural examinations of bilayer composites suggest that γ-$Al_{12}Mg_{17}$ is the

first reaction product that originates at the interface between Al and Mg, followed by the formation of the β-Al_3Mg_2 phase.

The mechanical behavior of the composites has been examined using room-temperature compression tests. The formation of the intermetallic phases increases the yield and compressive strengths of the composites, but decreases their plastic deformation. The strengthening effect depends on the amount of intermetallics formed during the consolidation step and, as a result, the yield strength of the composites follows the iso-stress model when the data are plotted as a function of the cumulative volume percentage of the intermetallic reinforcement.

Author Contributions: R.N.S. and S.S. designed the experiments, analyzed and interpreted the data, and wrote the paper; R.N.S. synthesized and characterized the specimens.

Funding: This research was funded by the DAAD (Deutscher Akademischer Austauschdienst), Research Grants for Doctoral Programmes in Germany (57048249).

Acknowledgments: The authors thank Birgit Bartusch, Harald Merker and Tianbing He for technical assistance, and Jürgen Eckert for stimulating discussions.

Conflicts of Interest: The authors declare no conflict of interest.

References

1. Allison, J.E.; Cole, G.S. Metal-matrix composites in the automotive industry: Opportunities and challenges. *JOM* **1993**, *45*, 19–24. [CrossRef]
2. Immarigeon, J.P.; Holt, R.T.; Koul, A.K.; Zhao, L.; Wallace, W.; Beddoes, J.C. Lightweight materials for aircraft applications. *Mater. Charact.* **1995**, *35*, 41–67. [CrossRef]
3. Jambor, A.; Beyer, M. New cars—New materials. *Mater. Des.* **1997**, *18*, 203–209. [CrossRef]
4. Cole, G.S.; Sherman, A.M. Light weight materials for automotive applications. *Mater. Charact.* **1995**, *35*, 3–9. [CrossRef]
5. González Palencia, J.C.; Furubayashi, T.; Nakata, T. Energy use and CO_2 emissions reduction potential in passenger car fleet using zero emission vehicles and lightweight materials. *Energy* **2012**, *48*, 548–565. [CrossRef]
6. Evans, A.G. Lightweight materials and structures. *MRS Bull.* **2013**, *26*, 790–797. [CrossRef]
7. Bodunrin, M.O.; Alaneme, K.K.; Chown, L.H. Aluminium matrix hybrid composites: A review of reinforcement philosophies; mechanical, corrosion and tribological characteristics. *J. Mater. Res. Technol.* **2015**, *4*, 434–445. [CrossRef]
8. Kainer, K.U. *Metal Matrix Composites Custom-Made Materials for Automotive and Aerospace Engineering*; Wiley: Weinheim, Germany, 2006.
9. Lesuer, D.R.; Kipouros, G.J. Lightweight materials for transportation applications. *JOM* **1995**, *47*, 17. [CrossRef]
10. Kaufman, J.G.; Rooy, E.L. *Aluminum Alloy Castings: Properties, Processes, and Applications*; ASM International: Materials Park, Novelty, OH, USA, 2004.
11. Mordike, B.L.; Ebert, T. Magnesium: Properties—Applications—Potential. *Mater. Sci. Eng. A* **2001**, *302*, 37–45. [CrossRef]
12. Fukuda, H.; Kondoh, K.; Umeda, J.; Fugetsu, B. Fabrication of magnesium based composites reinforced with carbon nanotubes having superior mechanical properties. *Mater. Chem. Phys.* **2011**, *127*, 451–458. [CrossRef]
13. Chawla, N.; Chawla, K.K. *Metal Matrix Composites*; Springer: New York, NY, USA, 2006.
14. Miracle, D. Metal matrix composites—From science to technological significance. *Comp. Sci. Technol.* **2005**, *65*, 2526–2540. [CrossRef]
15. Chua, B.W.; Lu, L.; Lai, M.O. Deformation behaviour of ultrafine and nanosize-grained Mg alloy synthesized via mechanical alloying. *Philos. Mag.* **2006**, *86*, 2919–2939. [CrossRef]
16. Han, B.Q.; Lavernia, E.J.; Mohamed, F.A.; Bampton, C.C. Improvement of toughness and ductility of a cryomilled Al-Mg alloy via microstructural modification. *Metall. Mater. Trans. A* **2005**, *36*, 2081–2091. [CrossRef]
17. Cao, G.; Konishi, H.; Li, X. Mechanical properties and microstructure of Mg/SiC nanocomposites fabricated by ultrasonic cavitation based nanomanufacturing. *J. Manuf. Sci. Eng.* **2008**, *130*, 031105. [CrossRef]

18. Xiao, J.; Shu, D.W.; Wang, X.J. Effect of strain rate and temperature on the mechanical behavior of magnesium nanocomposites. *Int. J. Mech. Sci.* **2014**, *89*, 381–390. [CrossRef]
19. Clyne, T.W.; Withers, P.J. *An Introduction to Metal Matrix Composites (Cambridge Solid State Science Series)*; Cambridge University Press: Cambridge, UK, 1993.
20. Tan, M.J.; Zhang, X. Powder metal matrix composites: Selection and processing. *Mater. Sci. Eng. A* **1998**, *244*, 80–85. [CrossRef]
21. Jiang, Q.C.; Wang, H.Y.; Ma, B.X.; Wang, Y.; Zhao, F. Fabrication of B_4C particulate reinforced magnesium matrix composite by powder metallurgy. *J. Alloys Compd.* **2005**, *386*, 177–181. [CrossRef]
22. Scudino, S.; Liu, G.; Prashanth, K.G.; Bartusch, B.; Surreddi, K.B.; Murty, B.S.; Eckert, J. Mechanical properties of Al-based metal matrix composites reinforced with Zr-based glassy particles produced by powder metallurgy. *Acta Mater.* **2009**, *57*, 2029–2039. [CrossRef]
23. Ling, Y.; Hua, H.; Yuhong, Z.; Xiaomin, Y. Microstructure and mechanical properties of squeeze casting quasicrystal reinforced AZ91D magnesium matrix composites. *Rare Metal Mater. Eng.* **2016**, *45*, 1978–1982. [CrossRef]
24. Wan, D.; Yang, G.; Zhu, M.; Xu, Q.; Zhou, Y. Solidification of Mg-28%Zn-2%Y alloy involving icosahedral quasicrystal phase. *Trans. Nonferrous Met. Soc. China* **2007**, *17*, 586–589. [CrossRef]
25. Dubois, J.-M.; Belin-Ferre, E.; Urban, K. *Complex Metallic Alloys: Fundamentals and Applications*, 1st ed.; Wiley: Weinheim, Germany, 2011; p. 434.
26. Scudino, S.; Sakaliyska, M.; Surreddi, K.B.; Ali, F.; Eckert, J. Structure and mechanical properties of Al–Mg alloys produced by copper mold casting. *J. Alloys Compd.* **2010**, *504*, S483–S486. [CrossRef]
27. Yang, C.; Zhang, B.; Zhao, D.; Li, X.; Zhai, T.; Han, Q.; Liu, F. In-situ synthesis of AlN/Mg-Al composites with high strength and high plasticity. *J. Alloys Compd.* **2017**, *699*, 627–632. [CrossRef]
28. Contreras, A.; Angeles-Chávez, C.; Flores, O.; Perez, R. Structural, morphological and interfacial characterization of Al-Mg/TiC composites. *Mater. Charact.* **2007**, *58*, 685–693. [CrossRef]
29. Sharifi, H.; Ostovan, K.; Tayebi, M.; Rajaee, A. Dry sliding wear behavior of open-cell Al-Mg/Al_2O_3 and Al-Mg/SiC-Al_2O_3 composite preforms produced by a pressureless infiltration technique. *Tribol. Int.* **2017**, *116*, 244–255. [CrossRef]
30. Zhao, Y.; Ding, Z.; Chen, Y. Crystallographic orientations of intermetallic compounds of a multi-pass friction stir processed Al/Mg composite materials. *Mater. Charact.* **2017**, *128*, 156–164. [CrossRef]
31. Hou, L.; Li, B.; Wu, R.; Cui, L.; Ji, P.; Long, R.; Zhang, J.; Li, X.; Dong, A.; Sun, B. Microstructure and mechanical properties at elevated temperature of Mg-Al-Ni alloys prepared through powder metallurgy. *J. Mater. Sci. Tech.* **2017**, *33*, 947–953. [CrossRef]
32. Lu, L.; Zhang, Y.F. Influence of process control agent on interdiffusion between Al and Mg during mechanical alloying. *J. Alloys Compd.* **1999**, *290*, 279–283. [CrossRef]
33. Chen, J.; Bao, C.; Chen, W.; Zhang, L.; Liu, J. Mechanical properties and fracture behavior of Mg-Al/AlN composites with different particle contents. *J. Mater. Sci. Tech.* **2017**, *33*, 668–674. [CrossRef]
34. Chen, J.; Bao, C.; Chen, F. Evolutions of microstructure and mechanical properties for Mg-Al/AlN composites under hot extrusion. *Mater. Sci. Eng. A* **2016**, *667*, 426–434. [CrossRef]
35. Bohn, R.; Haubold, T.; Birringer, R.; Gleiter, H. Nanocrystalline intermetallic compounds—An approach to ductility? *Scr. Metall. Mater.* **1991**, *25*, 811–816. [CrossRef]
36. Deevi, S.C.; Sikka, V.K. Nickel and iron aluminides: An overview on properties, processing, and applications. *Intermetallics* **1996**, *4*, 357–375. [CrossRef]
37. Davis, J.R. Aluminum and aluminum alloys. In *ASM Specialty Handbook*; ASM International: Materials Park, Novelty, OH, USA, 1993.
38. Tjong, S.C.; Ma, Z.Y. Microstructural and mechanical characteristics of in situ metal matrix composites. *Mater. Sci. Eng. R* **2000**, *29*, 49–113. [CrossRef]
39. Tang, F.; Anderson, I.E.; Gnaupel-Herold, T.; Prask, H. Pure Al matrix composites produced by vacuum hot pressing: Tensile properties and strengthening mechanisms. *Mater. Sci. Eng. A* **2004**, *383*, 362–373. [CrossRef]
40. Lee, M.H.; Kim, J.H.; Park, J.S.; Kim, J.C.; Kim, W.T.; Kim, D.H. Fabrication of Ni–Nb–Ta metallic glass reinforced al-based alloy matrix composites by infiltration casting process. *Scr. Mater.* **2004**, *50*, 1367–1371. [CrossRef]

41. Khodabakhshi, F.; Simchi, A.; Kokabi, A.H.; Gerlich, A.P. Friction stir processing of an aluminum-magnesium alloy with pre-placing elemental titanium powder: In-situ formation of an Al_3Ti-reinforced nanocomposite and materials characterization. *Mater. Charact.* **2015**, *108*, 102–114. [CrossRef]
42. Hashim, J.; Looney, L.; Hashmi, M.S.J. Particle distribution in cast metal matrix composites—Part I. *J. Mater. Process. Technol.* **2002**, *123*, 251–257. [CrossRef]
43. Ali, F.; Scudino, S.; Anwar, M.S.; Shahid, R.N.; Srivastava, V.C.; Uhlenwinkel, V.; Stoica, M.; Vaughan, G.; Eckert, J. Al-based metal matrix composites reinforced with Al-Cu-Fe quasicrystalline particles: Strengthening by interfacial reaction. *J. Alloys Compd.* **2014**, *607*, 274–279. [CrossRef]
44. Shahid, R.N.; Scudino, S. Microstructural strengthening by phase transformation in Al-Fe_3Al composites. *J. Alloys Compd.* **2017**, *705*, 590–597. [CrossRef]
45. Mallick, A. Improvement of mechanical properties in light weight Mg-based materials. *Procedia Eng.* **2016**, *149*, 283–287. [CrossRef]
46. Fang, C.; Wang, L.; Hao, H.; Zhang, X. Distribution of TiB_2 reinforcements in magnesium matrix composites by a multi-physical coupling field. *J. Mater. Process. Technol.* **2014**, *214*, 551–555. [CrossRef]
47. Liu, Z.; Han, Q.; Li, J.; Huang, W. Effect of ultrasonic vibration on microstructural evolution of the reinforcements and degassing of in situ TiB_{2P}/Al–12Si–4Cu composites. *J. Mater. Process. Technol.* **2012**, *212*, 365–371. [CrossRef]
48. Pitkethly, M.J. Nanomaterials—The driving force. *Mater. Today* **2004**, *7*, 20–29. [CrossRef]
49. Garcés, G.; Domínguez, F.; Pérez, P.; Caruana, G.; Adeva, P. Effect of extrusion temperature on the microstructure and plastic deformation of PM-AZ92. *J. Alloys Compd.* **2006**, *422*, 293–298. [CrossRef]
50. Nakashima, K.; Iwasaki, H.; Mori, T.; Mabuchi, M.; Nakamura, M.; Asahina, T. Mechanical properties of a powder metallurgically processed Mg-5Y-6Re alloy. *Mater. Sci. Eng. A* **2000**, *293*, 15–18. [CrossRef]
51. Lü, L.; Lai, M.O.; Liang, W. Magnesium nanocomposite via mechanochemical milling. *Comp. Sci. Technol.* **2004**, *64*, 2009–2014. [CrossRef]
52. Torralba, J.M.; da Costa, C.E.; Velasco, F. P/M aluminum matrix composites: An overview. *J. Mater. Process. Technol.* **2003**, *133*, 203–206. [CrossRef]
53. Harrigan, W.C. Commercial processing of metal matrix composites. *Mater. Sci. Eng. A* **1998**, *244*, 75–79. [CrossRef]
54. Das, D.K.; Mishra, P.C.; Singh, S.; Pattanaik, S. Fabrication and heat treatment of ceramic-reinforced aluminium matrix composites—A review. *Int. J. Mech. Mater. Eng.* **2014**, *9*, 6. [CrossRef]
55. Das, D.K.; Mishra, P.C.; Singh, S.; Thakur, R.K. Properties of ceramic-reinforced aluminium matrix composites—A review. *Int. J. Mech. Mater. Eng.* **2014**, *9*, 12. [CrossRef]
56. Long, R.A. *Fabrication and Properties of Hot-Pressed Molybdenum Disilicide*; Lewis Flight Propulsion Lab, National Advisory Committee for Aeronautics (NACA): Washington, DC, USA, 1950.
57. Huffadine, J.B. The fabrication and properties of molybdenum disilicide and molybdenum disilicide–alumina. In *Special Ceramics*; Proper, P., Ed.; Academic Press: New York, USA, 1960; pp. 220–236.
58. Smith, E. Macro process for direct production of tungsten monocarbide. *Met. Powder Rep. Met. Powder Rep.* **1979**, *35*, 53.
59. Coble, R.L. Reactive sintering. In *Sintering-Theory and Practice*; Kolar, D., Pejovnik, S., Ristic, M., Eds.; Elsevier Scientific Publishing Co.: Amsterdam, The Netherlands, 1982; p. 145.
60. Eisen, W.; Ferguson, B.; German, R.; Iacocca, R.; Lee, P.; Madan, D.; Moyer, K.; Sanderow, H.; Trudel, Y. *Powder Metal Technologies and Applications*; OSTI. GOV: Oak Ridge, TN, USA, 1998.
61. Dunand, D.C. Reactive synthesis of aluminide intermetallics. *Mater. Manuf. Proc.* **1995**, *10*, 373–403. [CrossRef]
62. Alman, D. Powder fabrication of monolithic and composite NiAl. *IJPM* **1991**, *27*, 29–41.
63. Fahrenholtz, W.; Ewsuk, K.; Loehmann, R.; Tomasia, A. In-situ reactions for synthesis of composites, ceramics and intermetallics. *Miner. Met. Mater. Soc. Warrenda* **1995**, *99*, 327–342.
64. Horton, J.; Baker, I.; Hanada, S.; Noebe, R.D.; Schwartz, D.S. *High-Temperature Ordered Intermetallic Alloys VI*; Materials Research Scociety: Pittsburgh, PA, USA, 1994.
65. Zhang, H.; Zhao, Y.; Yan, Y.; Fan, J.; Wang, L.; Dong, H.; Xu, B. Microstructure evolution and mechanical properties of mg matrix composites reinforced with al and nano SiC particles using spark plasma sintering followed by hot extrusion. *J. Alloys Compd.* **2017**, *725*, 652–664. [CrossRef]

66. Förster, W.; Binotsch, C.; Awiszus, B.; Dietrich, D.; Nickel, D. Interface engineering of aluminum-magnesium compounds. *Mater. Today Proc.* **2015**, *2*, 3–8. [CrossRef]
67. Kittner, K.; Feuerhack, A.; Förster, W.; Binotsch, C.; Graf, M. Recent developments for the production of Al-Mg compounds. *Mater. Today Proc.* **2015**, *2*, S225–S232. [CrossRef]
68. Li, C.; Chi, C.; Lin, P.; Zhang, H.; Liang, W. Deformation behavior and interface microstructure evolution of Al/Mg/Al multilayer composite sheets during deep drawing. *Mater. Des.* **2015**, *77*, 15–24. [CrossRef]
69. Skorpen, K.G.; Mauland, E.; Reiso, O.; Roven, H.J. Novel method of screw extrusion for fabricating Al/Mg (macro-) composites from aluminum alloy 6063 and magnesium granules. *Trans. Nonferrous Met. Soc. China* **2014**, *24*, 3886–3893. [CrossRef]
70. Guo, B.; Yi, J.; Ni, S.; Shen, R.; Song, M. Factors affecting the microstructure and mechanical properties of Ti-Al_3Ti core-shell-structured particle-reinforced Al matrix composites. *Philos. Mag.* **2016**, *96*, 1197–1211. [CrossRef]
71. Lee, J.-M.; Kang, S.B.; Sato, T.; Tezuka, H.; Kamio, A. Fabrication of Al/Al_3Fe composites by plasma synthesis method. *Mater. Sci. Eng.* **2003**, *A343*, 199–209. [CrossRef]
72. Laplanche, G.; Joulain, A.; Bonneville, J.; Schaller, R.; El Kabir, T. Microstructures and mechanical properties of Al-base composite materials reinforced by Al-Cu-Fe particles. *J. Alloys Compd.* **2010**, *493*, 453–460. [CrossRef]
73. Qi, N.; Hu, M.; Wang, Z.; Lu, Z.; Xie, C. Synthesis of Al/Fe_3Al core-shell intermetallic nanoparticles by chemical liquid deposition method. *Adv. Powder Technol.* **2013**, *24*, 926–931. [CrossRef]
74. Wang, Y.; Song, M.; Ni, S.; Xue, Y. In situ formed core-shell structured particle reinforced aluminum matrix composites. *Mater. Des.* **2014**, *56*, 405–408. [CrossRef]
75. Xue, Y.; Shen, R.; Ni, S.; Xiao, D.; Song, M. Effects of sintering atmosphere on the mechanical properties of Al-Fe particle-reinforced Al-based composites. *J. Mater. Eng. Perform.* **2015**, *24*, 1890–1896. [CrossRef]
76. Azizieh, M.; Mazaheri, M.; Balak, Z.; Kafashan, H.; Kim, H.S. Fabrication of Mg/$Al_{12}Mg_{17}$ in-situ surface nanocomposite via friction stir processing. *Mater. Sci. Eng. A* **2018**, *712*, 655–662. [CrossRef]
77. Brennan, S.; Bermudez, K.; Kulkarni, N.S.; Sohn, Y. Interdiffusion in the Mg-Al system and intrinsic diffusion in β-Mg_2Al_3. *Metall. Mater. Trans. A* **2012**, *43*, 4043–4052. [CrossRef]
78. Wang, J.; Li, Y.; Huang, W. Interface microstructure and diffusion kinetics in diffusion bonded Mg/Al joint. *React. Kinet. Catal. Lett.* **2008**, *95*, 71–79. [CrossRef]
79. Seyyed Afghahi, S.S.; Jafarian, M.; Paidar, M.; Jafarian, M. Diffusion bonding of Al 7075 and Mg AZ31 alloys: Process parameters, microstructural analysis and mechanical properties. *Trans. Nonferrous Met. Soc. China* **2016**, *26*, 1843–1851. [CrossRef]
80. Liu, W.; Long, L.; Ma, Y.; Wu, L. Microstructure evolution and mechanical properties of Mg/Al diffusion bonded joints. *J. Alloys Compd.* **2015**, *643*, 34–39. [CrossRef]
81. Dietrich, D.; Nickel, D.; Krause, M.; Lampke, T.; Coleman, M.P.; Randle, V. Formation of intermetallic phases in diffusion-welded joints of aluminium and magnesium alloys. *J. Mater. Sci.* **2011**, *46*, 357–364. [CrossRef]
82. Su, H.L.; Harmelin, M.; Donnadieu, P.; Baetzner, C.; Seifert, H.J.; Lukas, H.L.; Effenberg, G.; Aldinger, F. Experimental investigation of the Mg-Al phase diagram from 47 to 63 at % Al. *J. Alloys Compd.* **1997**, *247*, 57–65. [CrossRef]
83. Panteli, A.; Robson, J.D.; Brough, I.; Prangnell, P.B. The effect of high strain rate deformation on intermetallic reaction during ultrasonic welding aluminium to magnesium. *Mater. Sci. Eng. A* **2012**, *556*, 31–42. [CrossRef]
84. Lee, K.S.; Kim, J.S.; Jo, Y.M.; Lee, S.E.; Heo, J.; Chang, Y.W.; Lee, Y.S. Interface-correlated deformation behavior of a stainless steel-Al-Mg 3-ply composite. *Mater. Charact.* **2013**, *75*, 138–149. [CrossRef]
85. Negendank, M.; Mueller, S.; Reimers, W. Coextrusion of Mg-Al macro composites. *J. Mater. Process. Technol.* **2012**, *212*, 1954–1962. [CrossRef]
86. Njiokep, T.; Eugene, M.; Salamon, M.; Mehrer, H. Growth of Intermetallic Phases in the Al-Mg System. In *Defect and Diffusion Forum*; Trans. Tech. Publ.: Zürich, Switzerland, 2001; pp. 1581–1586.
87. Funamizu, Y.; Watanabe, K. Interdiffusion in the Al–Mg system. *Trans. Jpn. Inst. Met.* **1972**, *13*, 278–283. [CrossRef]
88. Laidler, K.J. *Chemical Kinetics*, 3rd ed.; Harper Collins: NewYork, NY, USA, 1987.
89. Svoboda, J.; Fischer, F.D. Incorporation of vacancy generation/annihilation into reactive diffusion concept—Prediction of possible kirkendall porosity. *Comp. Mater. Sci.* **2017**, *127*, 136–140. [CrossRef]

90. Bhadeshia, H. The Kirkendall Effect. Available online: http://www.msm.cam.ac.uk/phase-trans/kirkendall.html (accessed on 13 April 2018).
91. ASTM E6-03. *Standard Terminology Relating to Methods of Mechanical Testing, Annual Book of ASTM Standards*; ASTM international: West Conshohocken, PA, USA, 2003.
92. Scudino, S.; Surreddi, K.B.; Sager, S.; Sakaliyska, M.; Kim, J.S.; Löser, W.; Eckert, J. Production and mechanical properties of metallic glass-reinforced Al-based metal matrix composites. *J. Mater. Sci.* **2008**, *43*, 4518–4526. [CrossRef]
93. Chawla, K.K. *Composite Materials: Science and Engineering*; Springer: New York, NY, USA, 1987.
94. Kim, H.S. On the rule of mixtures for the hardness of particle reinforced composites. *Mater. Sci. Eng. A* **2000**, *289*, 30–33. [CrossRef]
95. Kim, H.S.; Hong, S.I.; Kim, S.J. On the rule of mixtures for predicting the mechanical properties of composites with homogeneously distributed soft and hard particles. *J. Mater. Process. Technol.* **2001**, *112*, 109–113. [CrossRef]
96. Kim, J.Y.; Scudino, S.; Kühn, U.; Kim, B.S.; Lee, M.H.; Eckert, J. Production and characterization of brass-matrix composites reinforced with $Ni_{59}Zr_{20}Ti_{16}Si_2Sn_3$ glassy particles. *Metals* **2012**, *2*, 79–94. [CrossRef]
97. Li, Z.; Schmauder, S.; Dong, M. A simple mechanical model to predict fracture and yield strengths of particulate two-phase materials. *Comp. Mater. Sci.* **1999**, *15*, 11–21. [CrossRef]
98. Wang, Z.; Scudino, S.; Stoica, M.; Zhang, W.; Eckert, J. Al-based matrix composites reinforced with short Fe-based metallic glassy fiber. *J. Alloys Compd.* **2015**, *651*, 170–175. [CrossRef]
99. Singh, A.; Solanki, K.; Manuel, M.; Neelameggham, N. *Magnesium Technology*; Springer International Publishing: New York, NY, USA, 2016.
100. Zolriasatein, A.; Khosroshahi, R.A.; Emamy, M.; Nemati, N. Mechanical and wear properties of Al-Al_3Mg_2 nanocomposites prepared by mechanical milling and hot pressing. *Int. J. Min. Met. Mater.* **2013**, *20*, 290–297. [CrossRef]
101. Scudino, S.; Liu, G.; Sakaliyska, M.; Surreddi, K.B.; Eckert, J. Powder metallurgy of Al-based metal matrix composites reinforced with β-Al_3Mg_2 intermetallic particles: Analysis and modeling of mechanical properties. *Acta Mater.* **2009**, *57*, 4529–4538. [CrossRef]